Int. J. Electrochem. Sci., 11 **(2016)** 3007 - 3023

International Journal of
ELECTROCHEMICAL
SCIENCE
www.electrochemsci.org

Effect of Calcareous Sediments on Hydrogen Evolution Potential of 16Mn Steel in Seawater

Zhiming Gao[1,*], *Xiaoyu Liu*[1], *Lijuan Wen*[2], *Weiwei Kang*[1]

[1]School of Material Science and Technology, Tianjin University, Tianjin, 30072, China
[2]Technical Support Department, Hainan Nuclear Power Co., Ltd., Changjiang of Hainan Prov., 572733, China
[*]E-mail: gaozhiming@tju.edu.cn

Received: 30 December 2015 / *Accepted:* 3 February 2016 / *Published:* 1 March 2016

Effect of calcareous sediments on hydrogen evolution potential which formed under different cathodic protection potentials was investigated in this paper. Electrochemical impedance spectroscopy (EIS), potentiodynamic polarization and hydrogen permeation experiment were carried out to analyze the electrochemical properties of 16Mn steels covered with different calcareous sediments. The microstructures of different calcareous sediments were obtained by using three-dimensional microscope and scanning electron microscopy (SEM). It is concluded that, hydrogen evolution potentials of 16Mn steels covered with different calcium deposits shift negatively to different degrees. As pre-polarization potential turns negative, hydrogen evolution potential of 16Mn steels pre-treated turns negative constantly at first and then turns positive. The hydrogen evolution potential corresponding to pre-polarization potential at -1.05V is the lowest. Corresponding to the change of hydrogen evolution potential, applying pre-polarization ranging from -0.90V to -1.05V, the calcareous sediments obtained become thicker and thicker. Embossments of calcareous sediments increase gradually. Until applying the potential at -1.10v, the calcareous sediments are damaged. Mechanisms of the phenomenon that hydrogen evolution potential shifts negatively are as follows: one factor is the IR drop caused by calcareous sediments. Another factor is the calcareous sediments can hinder the diffusion of H_2 to solution and indirectly inhibit the hydrogen evolution reaction.

Keywords: calcareous sediments; hydrogen evolution potential; cathodic protection potential; hydrogen permeation current;

1. INTRODUCTION

Cathodic protection is a common anticorrosive method and indeed of great help to corrosion protection of metal [1-4]. For example, Crevice corrosion can be evitable because of cathodic protection and the mechanism was proposed [5]. Corrosive wear of 304 stainless steel caused by low

wearing force can also be avoided by applying an appropriate cathodic protection [6]. However, excessive cathodic protection can cause hydrogen embrittlement, which led to a decline in mechanics performance of materials. Nowadays a large number of researches have been carried out to study the relation between the cathodic protection and hydrogen embrittlement [7-10]. For example, the proper cathodic protection potential for the steel in marine environments was obtained by the slow stain rate test (SSRT) and SEM fractography analysis [11].

In addition, calcareous sediments can be obtained during the process of cathodic protection for the metal in seawater. What is more, applying different cathodic protection potentials on the steel in different solutions, the structure and composition of calcareous sediments is various [12, 13]. The calcareous sediments covered on the surface of the metal have the effect of protection and the role played by each kind of components such as $CaCO_3$ and $Mg(OH)_2$ was analyzed during the process of protection for metals [14-16]. The calcareous sediments can hinder the diffusion of oxygen to the surface of metals and alleviate oxygen reaction. In this paper, we mainly talk about whether calcareous sediments obtained under different cathodic protection potentiala can also have an effect on hydrogen evolution and change hydrogen evolution potential. Meanwhile, the influence mechanism is come out.

2. EXPERIMENT

2.1 Material

The material we used is 16Mn steel and its chemical composition can be seen from Table.1. The steel was made into specimen one (10x10x1mm) and specimen two (40x40x1mm). The specimen one was connected to a copper wire at one side to provide electrical contact and then embedded in epoxy resin, with an work area of 1cm^2. The surface of the specimen one was abraded with carbide paper (from 100# to 1500#) and they were ready for the operation after having been washed by distilled water, degreased by ethanol and dried by cool air. We plated nickel on one side of the specimen two after degreasing and acid activation to be the working electrode of Devanathan-Stackurski method [17].

Table 1. Chemical composition (wt. %) of 16Mn steel

C	Si	Mn	Cr	P	S	Ni	Cu
0.13～0.19	0.20～0.60	1.20～1.60	≤0.30	≤0.030	≤0.030	≤0.30	≤0.25

2.2 Potentiostatic Polarization

A three-electrode configuration was used for the experiment. The specimen one was used as the working electrode, the counter electrode was platinum sheet and the reference electrode was a saturated calomel electrode (SCE) with a salt bridge. The aqueous medium is the seawater in Tianjin.

Cathodic protection potentials varying from -0.9V, -0.95V, -1.00V, -1.05V to -1.10V were exerted on the specimen one respectively for 7d to get the steels covered with different calcareous sediments.

2.3 Polarization Curve

A three-electrode system was used for the experiment. But we selected the specimen covered with different calcareous sediments as working electrode. The cathodic polarization curve of 16Mn steel covered with different calcareous sediments was performed from OCP to -1.25V_{SCE} at a scan rate of 0.166mV/s. All the experiments were tested at the room temperature.

2.4 Hydrogen Permeation

Devnathan-Stachurski electrolytic cell was made to obtain the hydrogen permeation curves of 16Mn steel. The working electrode (WE) was specimen two. We used Hg/HgO electrode as reference electrode (RE) and titanium mesh as counter electrode (CE) in anode chamber which was full of 0.2mol/L KOH solution. We used SCE electrode as reference electrode and titanium mesh as counter electrode in cathodic chamber which was full of 3.5% NaCl. 0.2$V_{Hg/HgO}$ was applied to ionize hydrogen which diffused from cathodic chamber to anode chamber. The whole test process is shown as follow: constant potential about 0.2$V_{Hg/HgO}$ was applied on the anode side of the sample and when the measured density value of the background current of the anode side is reduced to 0.5μA/cm^2 or less, we exerted a given cathodic protection potential on the cathodic side of the sample [18]. The curve of hydrogen penetration current changing with time was obtained.

2.5 Microstructure Characterization

Three-dimensional microscope and scanning electron microscopy (SEM) were used to analyze surface morphology of the calcareous sediment; Energy dispersive X-ray analyzer (EDX) analyses were carried out to get composition of calcareous sediments.

2.6 Electrochemical impedance spectroscopy

EIS measurements were carried out using an EG&G Parstat 2273 electrochemical workstation. EIS measurements were performed with a 10mv amplitude signal and the applied frequency ranged from 100kHz to 0.01Hz. A three-electrode system was used with the specimen covered with different calcareous sediments as the working electrode (WE), a saturated calomel electrode (SCE, 0.242 V vs. SHE) as the reference electrode (RE) and the platinum as the counter electrode (CE). The test was conducted at room temperature of ($25^{\pm 2)}$°C.

3. RESULTS

3.1 Polarization Curve

The cathodic polarization curves of 16Mn steels which had been pre-polarized for 7d are shown in Fig.1. As we know, as the polarization potential turns negative, the change of polarization current density has three stages: polarization current density is increasing at first and this stage is under activation control; polarization current density has no significant change with the polarization potential shifting more negatively and this stage is under oxygen diffusion control; polarization current density begin to grow rapidly at the last stage which is under hydrogen evolution reaction control [19-22].

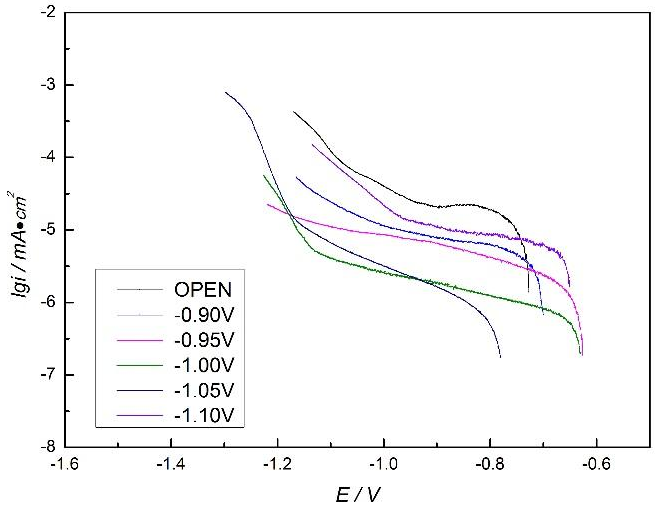

Figure 1. Polarization curves of 16Mn steels applying different pre-polarization potentials for 7d

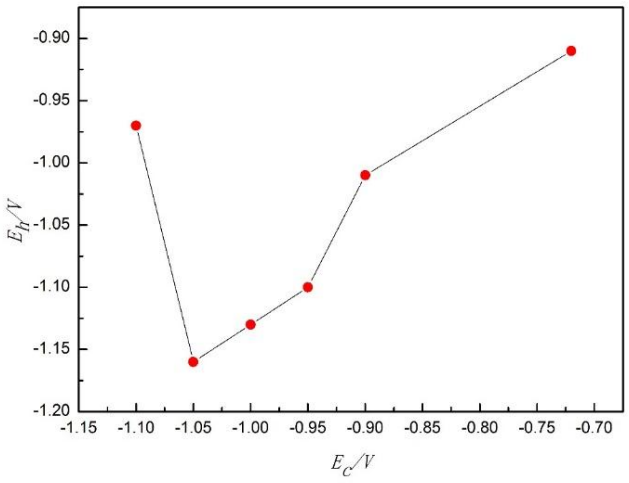

Figure 2. The relationship between hydrogen evolution potential (E_h) and pre-polarization potential(E_c)

The turning point can be seen between the second stage and the third stage and the corresponding potential is the hydrogen evolution potential. So the hydrogen evolution potentials of

16Mn steels covered with different calcareous sediments were got from Fig.1 and the relationship between hydrogen evolution potential ($\mathbf{E}_h$) and cathodic pre-polarization potential (E_c) was obtained in Fig.2. As pre-polarization potential shifts negatively, hydrogen evolution potential of 16Mn steels turns negative constantly at first and then turns positive. The hydrogen evolution potential corresponding to pre-polarization potential at -1.05V shifts most negatively.

3.2 Electrochemical Impedance Spectroscopy

Fig.3 shows the experimental and fitting results of EIS of 16Mn steels with different surface states at different cathodic potentials (-0.8V_{SCE} to -1.2V_{SCE}) in seawater. Two time constants can be inferred from the bode diagrams and the equivalent circuit is R(Q(R(QR))), shows in Fig.4, where $\mathbf{R}_s$ means the solution resistance, R_c is the resistance of the calcium deposits, $\mathbf{R}_t$ indicates the charge transfer resistance. Fig.3 shows the fitting curves have a good match with the experimental results. Meanwhile, the $\mathbf{R}_t$~E curves were obtained in Fig.5.

.

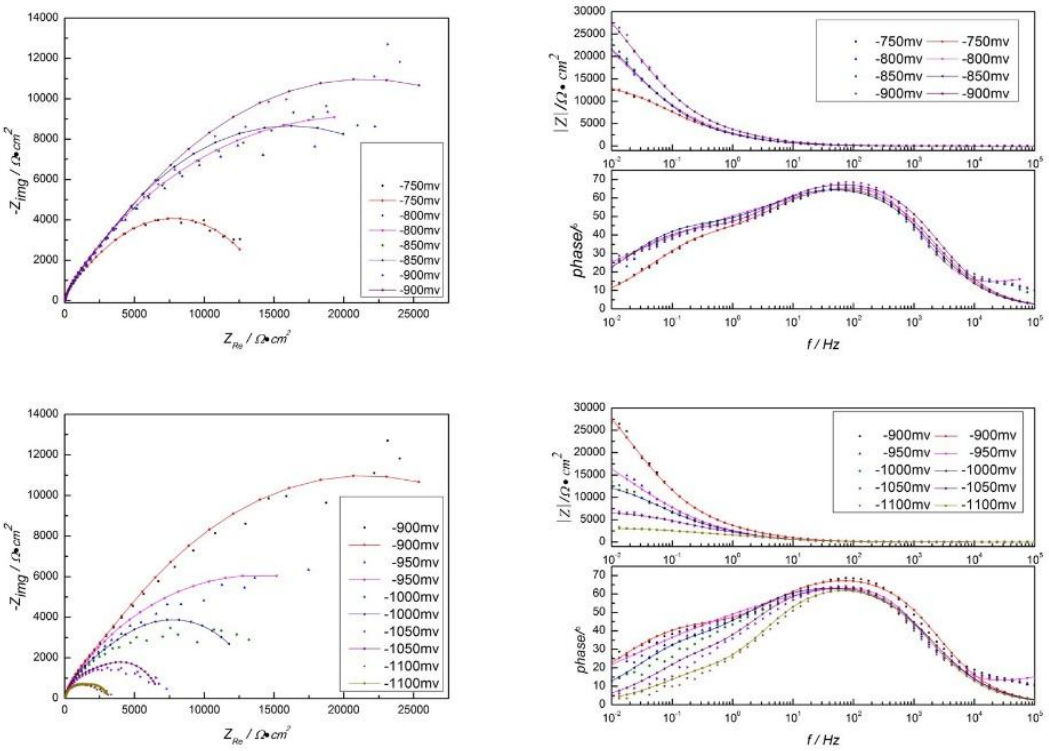

Figure 3-1. The EIS of 16Mn steel which had been pre-polarization for 7d under -0.90V

As we know, the charge transfer resistance changed with applied cathodic polarization potential. At the $\mathbf{E}_{corr}$ potential, there are two kinds of electrode reactions, anode reaction and cathode reaction. Therefore, the impedance measured in cathodic polarization potential is the comprehensive response to the anode and cathode reaction. At the mixed potentials, anodic and cathodic reactions occur simultaneously [18], so the charge transfer resistance of the impedance,$\mathbf{R}_t$, can be written as

$1/R_t = 1/Rt_a + 1/Rt_c$ (1)

Rt_a is the transfer resistance of anode reaction and Rt_c is the transfer resistance of cathode reactions.

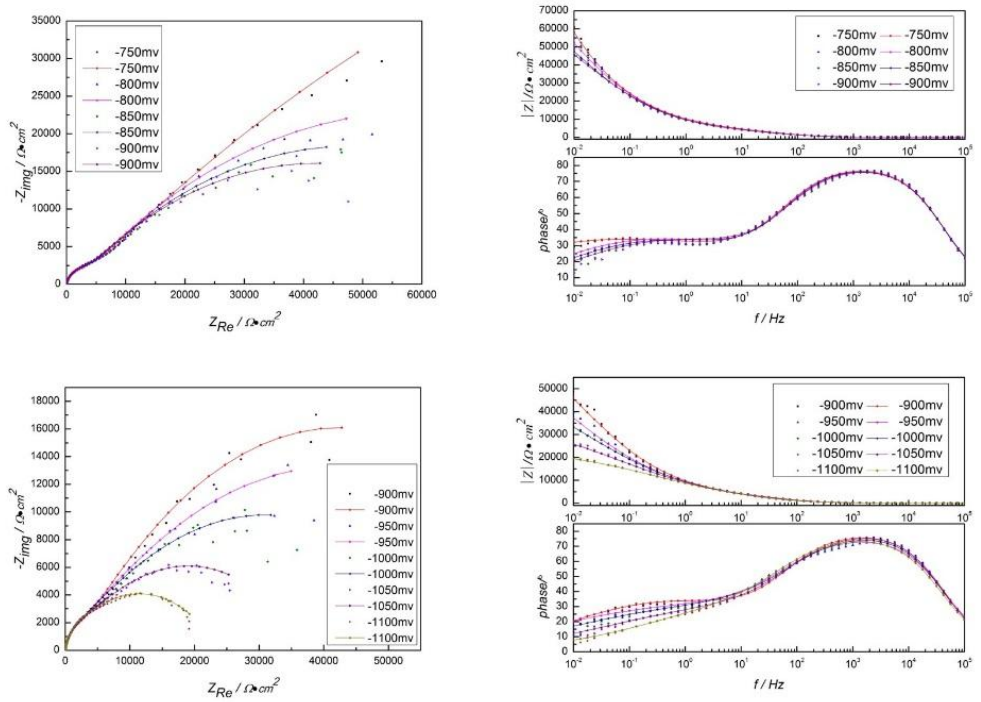

Figure 3-2. The EIS of 16Mn steel which had been pre-polarization for 7d under -0.95V

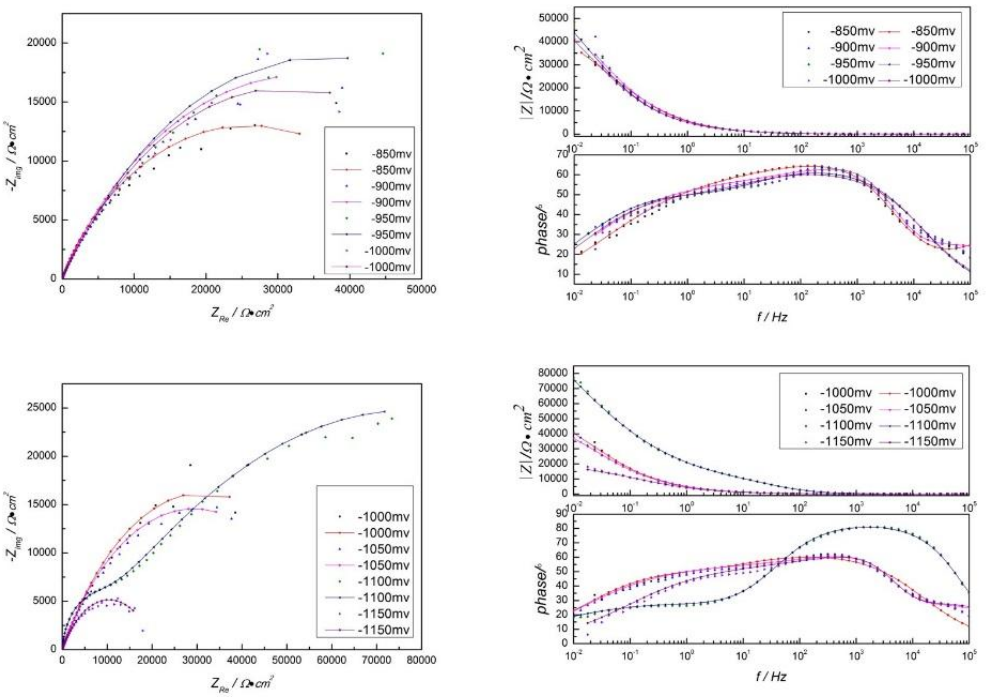

Figure 3-3. The EIS of 16Mn steel which had been pre-polarization for 7d under -1.00V

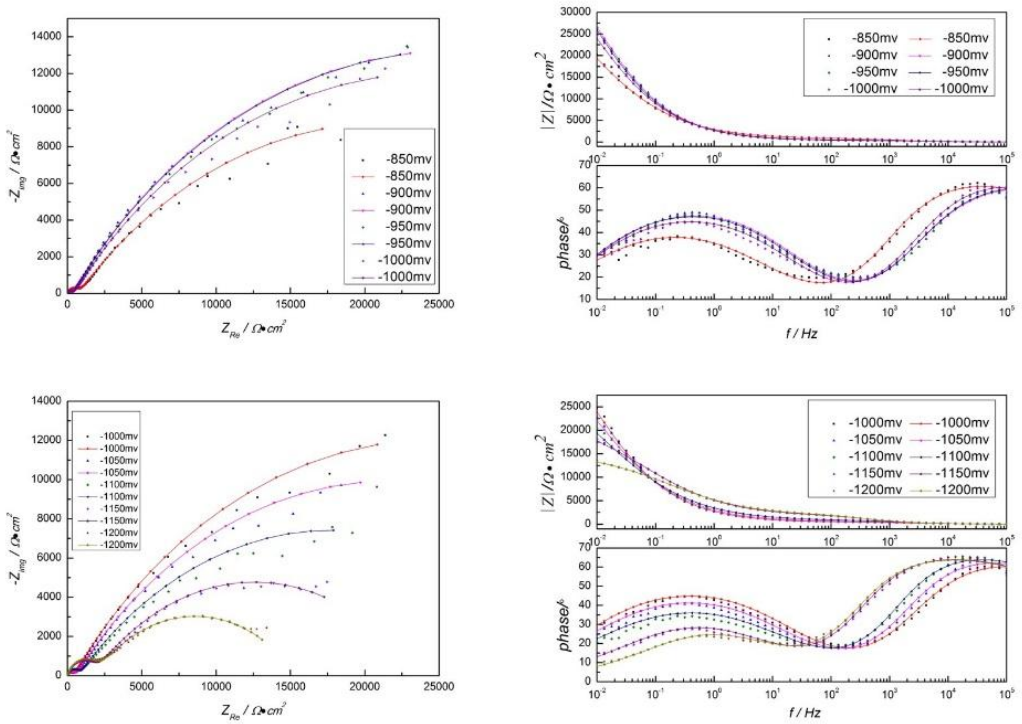

Figure 3-4. The EIS of 16Mn steel which had been pre-polarization for 7d under -1.05V

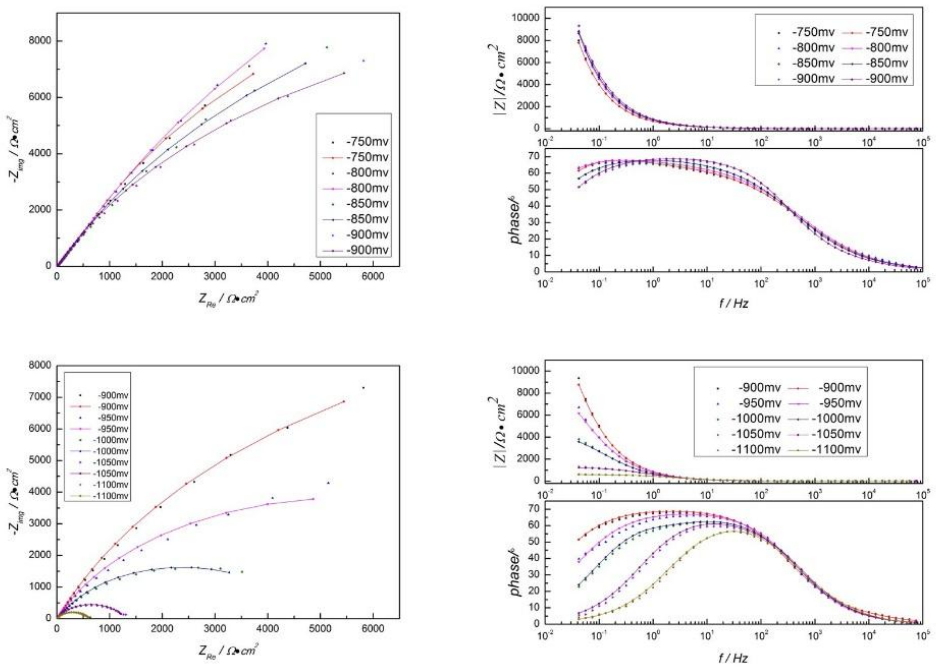

Figure 3-5. The EIS of 16Mn steel which had been pre-polarization for 7d under -1.10V

Figure 3. The EIS of 16Mn steel which had been pre-polarization for 7d under cathodic potentials ranging from -0.90V to -1.10V (Point diagrams are experimental results; Line diagrams mean fitting results)

When applied with cathodic polarization potential, Rt_a increases with the potential negatively shifting, while Rt_c reduces. When Rt_a is much larger than Rt_c, cathode reaction is the main reaction which occurred on the electrode surface. A suitable equivalent circuit was selected in Fig.6(a). In addition, when the cathodic polarization potential moved to a certain negative potential, together with oxygen reduction reaction, the hydrogen evolution reaction occurs. Another equivalent circuit used for modeling is shown in Fig.6(b). Rt_c, the transfer resistance of cathode, can be written as

$1/Rt_c=1/Rt_o+1/Rt_H$ (2)

Rt_o is the transfer resistance of oxygen reduction reaction and Rt_H is the transfer resistance of hydrogen evolution reaction.

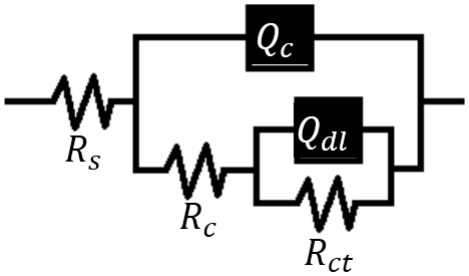

Figure 4. The fitting circuit

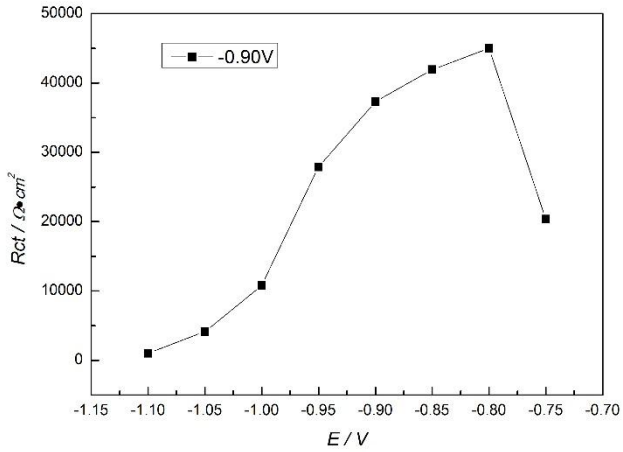

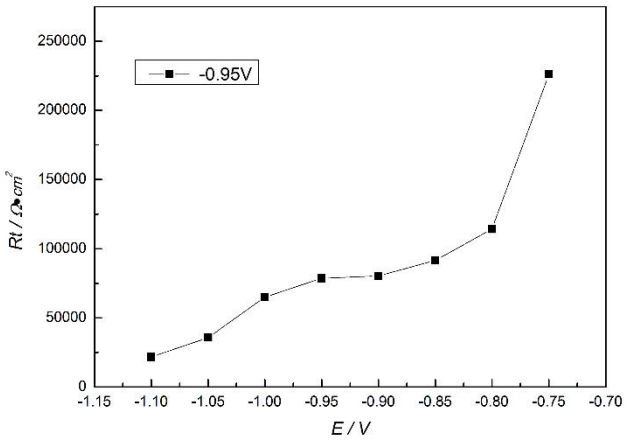

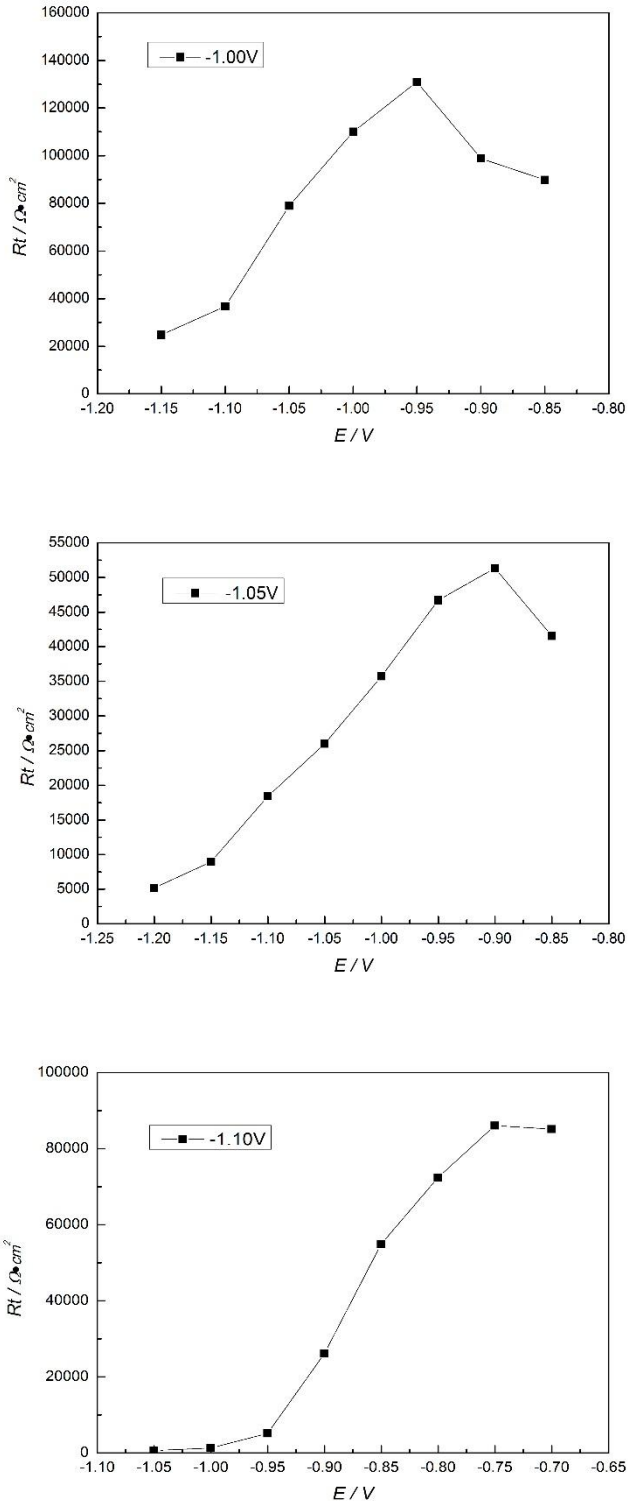

Figure 5. The curves of R_t changing with E

When the hydrogen evolution reaction makes up a small proportion in the cathodic reaction, $Rt_H \rightarrow \infty$, Rt_c is approximately equal to Rt_o. Rt_c decreased with the electrode potential becoming negative, so as the slope of Rt~E curve. When hydrogen reaction is obvious, Rt_H became smaller.

Rt_H, together with Rt_o reacted upon Rt_c. The declining rate of Rt_c changed because of Rt_H, causing a turning point in the Rt~E curve. The cathode potential of the inflection point is the hydrogen evolution potential. What is more, the hydrogen evolution potentials obtained by the Rt~E curves are consistent with those got by cathodic polarization curves, which is shown in Table. 2

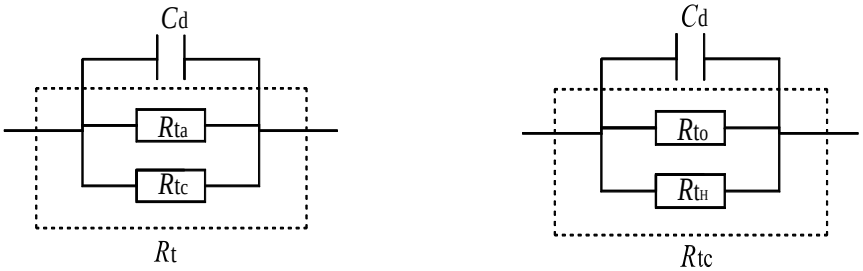

(a) **(b)**

Figure 6. Equivalent circuit ((a) used for modeling at mixed potential, (b) used for modeling under cathodic polarization)

Table 2. The hydrogen evolution potential obtained by two electrochemical methods

pre-polarization potential	E_h obtained by polarization curves	E_h obtained by the Rt~E curves
-0.90V	-1.01V	-1.00~-1.05V
-0.95V	-1.07V	-1.05~-1.10V
-1.00V	-1.13V	-1.10~-1.15V
-1.05V	-1.17V	-1.15~-1.20V
-1.10V	-0.96V	-0.95~-1.00V

3.3 Morphology

The morphology of calcareous sediments covered on the surface of the samples was observed by three-dimensional microscope. Fig. 7(a) shows that a relatively complete calcareous sedimentary layer with the maximum thickness of 8.085 microns formed on the surface of 16Mn steel pre-polarized under -0.90V and the layer is nearly no bubble; Fig. 7(b) shows that a complete calcareous sedimentary layer with the maximum thickness of 9.47 microns formed on the surface of 16Mn steel pre-polarized under -0.95V, but the layer presents some projections, indicating bubbles. Compared with Fig.7(b), Fig.7(c) shows that the layer presents more projections and the maximum thickness is 11.62 m; Fig.7(d) shows that calcareous sedimentary layer with the maximum thickness of 14.78 microns formed on the surface of 16Mn steel pre-polarized under -1.05V and the bubbles gathered as a piece; Fig.7(e) shows that the thickest calcareous sedimentary layer with the maximum thickness of 113 microns formed on the surface of 16Mn steel pre-polarized under -1.10V, but the layer have a very clear and dense projections.

Microstructure and composition of calcareous sediments obtained under different cathodic pre-polarized potentials was analyzed by SEM and EDX, which is shown in Fig.8. Grains of calcareous sediments obtained at -0.90V are big and stack up one piece by one piece (Fig.8(a)); Grains of

calcareous sediments obtained at -0.95V are bigger and some bulge (Fig.8(b));Compared to calcareous sediments obtained at -0.95V, calcareous sediments obtained at -1.00V bulge badly (Fig.8(c)); Grains of calcareous sediments obtained at -1.05V are embossment bonding together (Fig.8(d)); Grains of calcareous sediments obtained at -1.10V bump the worst (Fig.8e)).

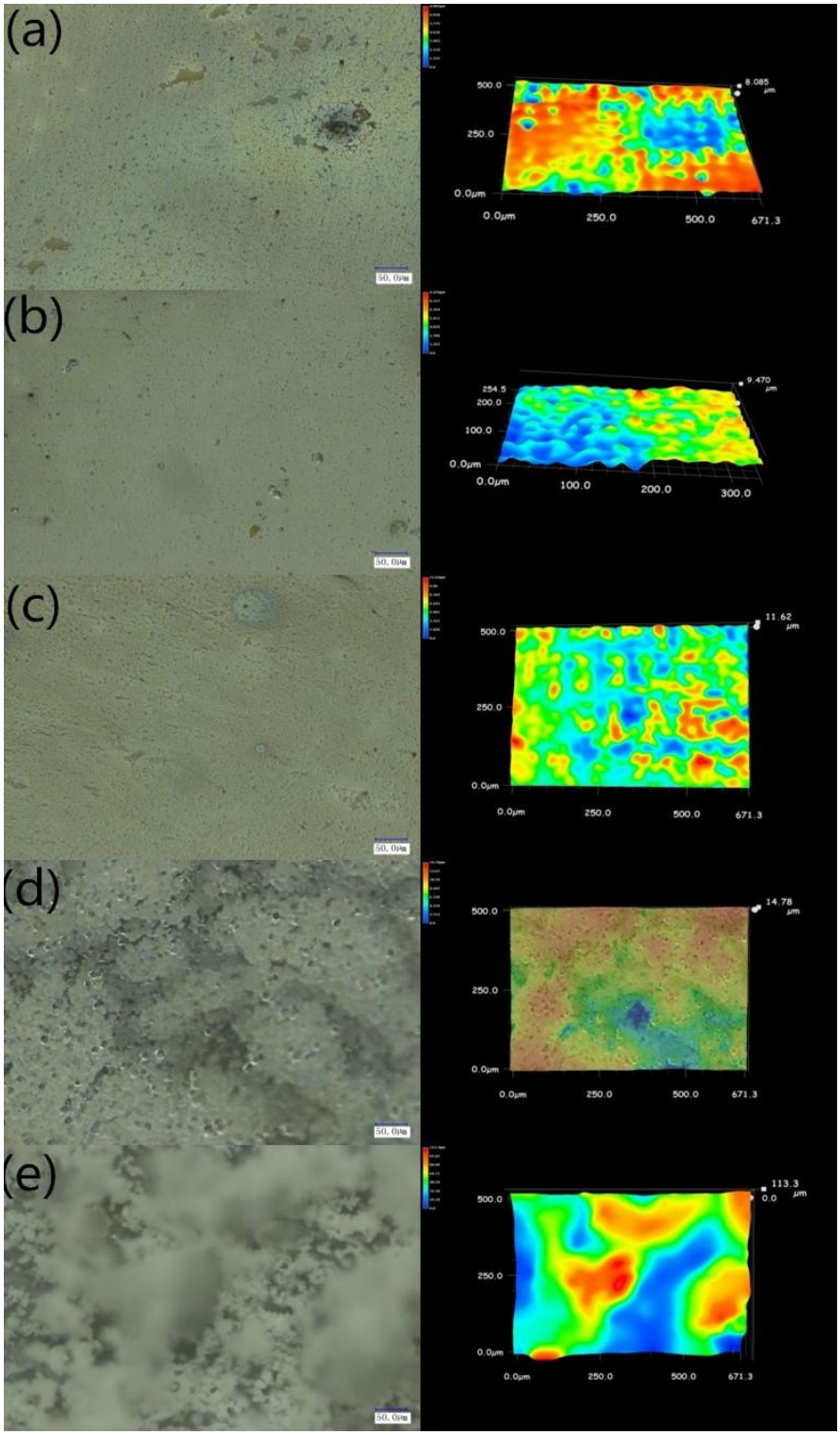

Figure 7. Three-dimensional morphology of 16Mn steel applying different pre-polarized potentials for 7d ((a) ~ (e) respectively represents morphology of 16Mn steels applying different pre-polarized potential ranging from -0.90V to 1.10V)

In all, the number of the bubble increases gradually and the area turns larger and larger. But the element of calcareous sediments are still calcium compound and little magnesium compound.

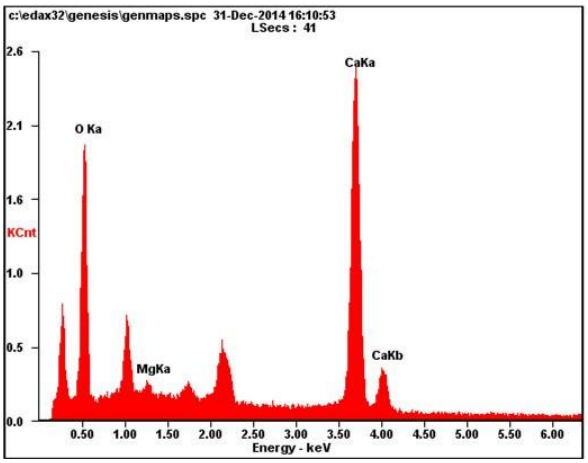

Element	Wt%	At%
OK	58.34	77.55
MgK	00.99	00.87
CaK	40.67	21.58
Matrix	Correction	ZAF

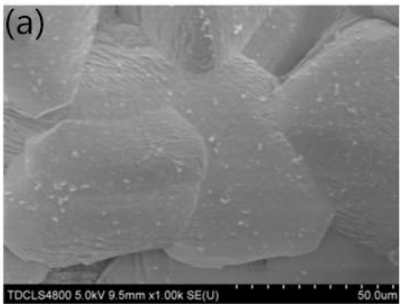

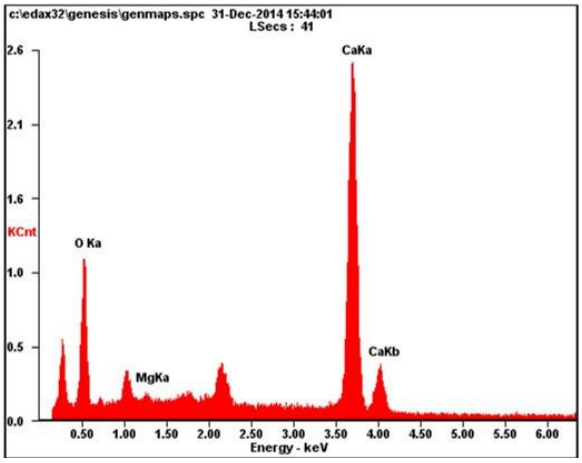

Element	Wt%	At%
OK	49.48	70.77
MgK	01.04	00.98
CaK	49.47	28.25
Matrix	Correction	ZAF

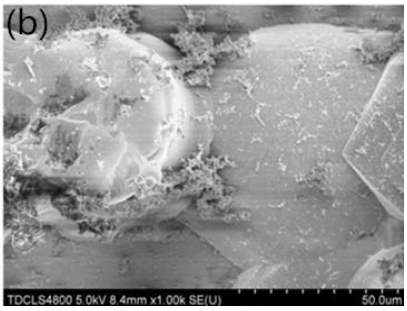

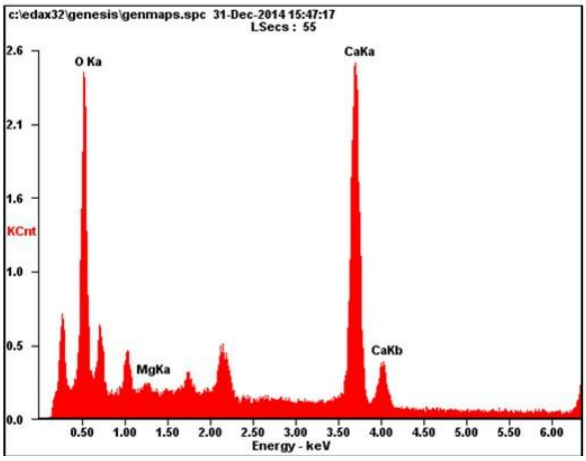

Element	Wt%	At%
OK	61.81	80.04
MgK	00.67	00.57
CaK	37.53	19.40
Matrix	Correction	ZAF

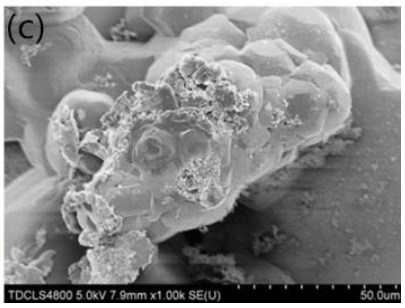

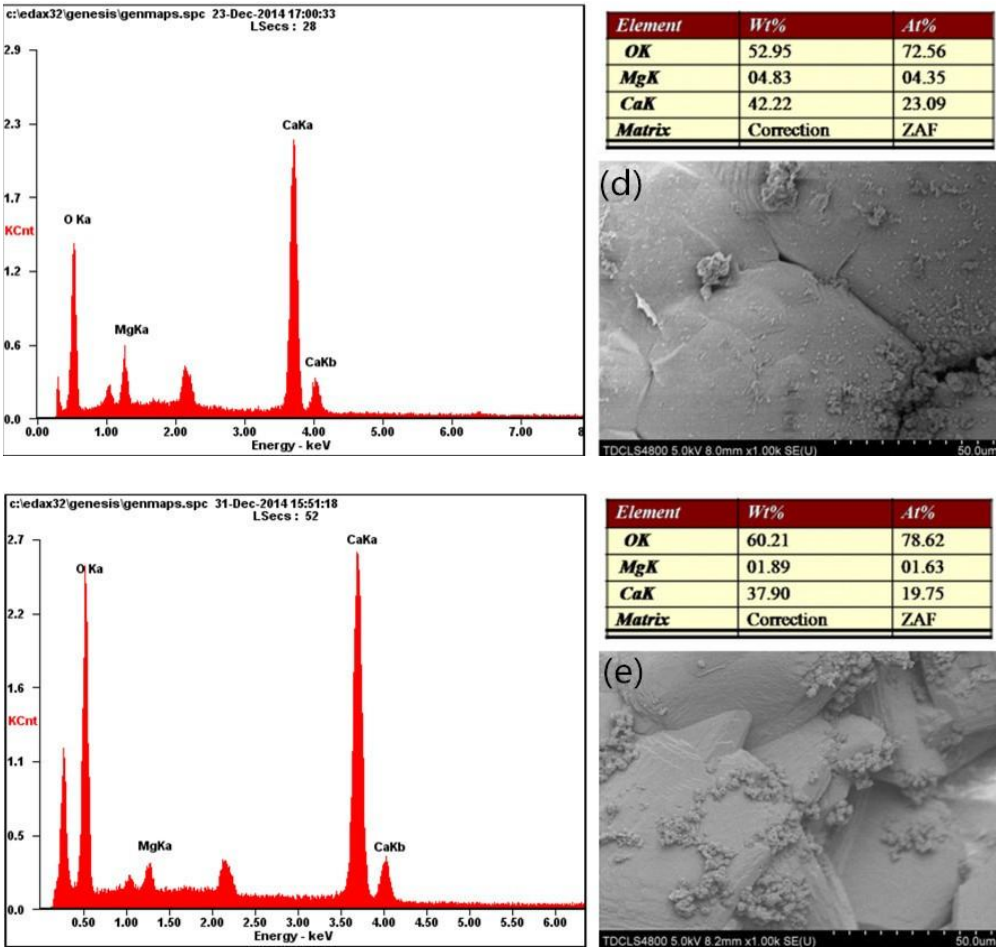

Figure 8. SEM and EDX of different calcareous deposits obtained by applying different pre-polarized potentials ranging from -0.90V to -1.10V ((a) ~ (e) respectively corresponds to -0.90V to 1.10V)

3.4 Hydrogen permeability

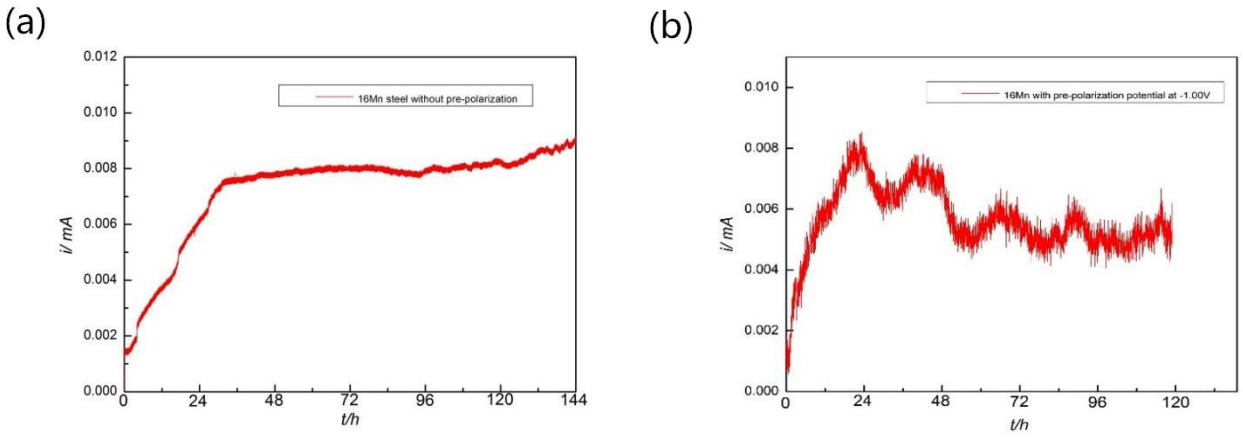

Figure 9. The curves of hydrogen penetration current changing with time ((a) 16Mn steel without pre-polarization, (b) 16Mn steel with pre-polarization potential at -1.00V)

The curves of hydrogen penetration current changing with time were obtained in Fig.9. The sample is 16Mn steel without pre-polarization in Fig.9 (a). Fig.9 (b) shows the current curve of 16Mn steel with pre-polarization potential at -1.00V.

The program shows hydrogen penetration current increases firstly and reaches the top for 1d. As time goes on, the current keeps stable. But for 16Mn steel with pre-polarization potential at -1.00V, as the time change, hydrogen penetration current also increases and reach the top. Stable for a period of time, the current begin to reduce until a certain value and then rise again;

4. DISCUSSION

Analyzing the measured polarization curve of the steel without pre-polarized in Fig.2, its hydrogen evolution potential is at about -0.91V. And so applying pre-polarization potential at -0.90V, calcium deposition layers formed is almost no bulge. Applying pre-polarization potential ranging from -0.95V to -1.10V, with potential negatively shifting, the rate of the formation of calcium deposition becomes faster and faster and the layers become thicker and thicker. The rate of hydrogen evolution reaction also becomes faster and faster and embossment caused by hydrogen bubble continues to increase. When hydrogen evolution reaction is weak, hydrogen bubbles will not lead to the damage of calcium deposition layers; Until the rate of the formation of hydrogen bubbles is fast enough to break the layer, calcareous sediments is no longer complete. It can be seen through the microstructure figures that applying pre-polarization potentials ranging from -0.95V to -1.05V, the films keep intact and applying -1.10V, the film breaks. In conclusion, different pre-polarization treatments led to different calcareous sediments, whose performance is also various [23, 24].

According to the cathodic polarization curves and Rt~E curves [10], a rule can be summarized that hydrogen evolution potential of 16Mn steel covered with different calcareous sediments negatively shifts to different degrees. As for the reason, the IR drop caused by calcareous sediments makes up a large proportion and can be seen in table 3. The actual polarization potential applied on the metal is positive than the polarization potential expected due to the IR drop [25]. E_{h1} is the hydrogen evolution potential after considering the IR drop. E_h is the hydrogen evolution potential obtained by experiment. There's a big difference between E_h and E_{h1}, which means another factor can also lead to hydrogen evolution potential negative shift.

Table 3. The IR drop caused by different calcareous sediments

	E_{corr}	-0.90V	-0.95V	-1.00V	-1.05V	-1.10V
$R_c(\Omega)$	-	3871	5713	7559	2004	348
i_c(A)	-	$7.98\text{x}10^{-6}$	$7.61\text{x}10^{-6}$	$1.33\text{x}10^{-5}$	$2.32\text{x}10^{-5}$	$5.03\text{x}10^{-5}$
IR(mv)	-	30.90	43.48	100.00	46.49	17.51
E_{h1}(mv)	0	-930.90	-943.48	-1000	-946.49	-917.51
E_h(mv)	-900	-1020	-1100	-1125	-1170	-960

There is such a phenomenon that as pre-polarization potential shifts negatively, hydrogen evolution potential of 16Mn steels pre-treated turns negative constantly at first and then turns positive. The hydrogen evolution potential corresponding to pre-polarization potential at -1.05V is the lowest. Combined with the analysis of the microstructure of calcium deposits, an inference was made and the mechanism picture can be seen in Fig.10.

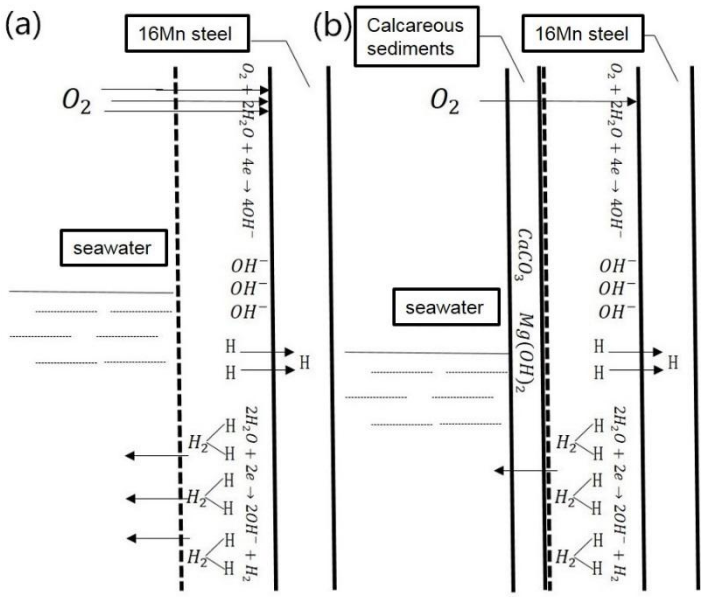

Figure 10. The mechanism picture ((a) 16Mn steel without calcareous sediments, (b) 16Mn steel with different calcareous sediments)

The calcium deposits film can hinder the diffusion of oxygen to protect the metal from corroding [26]. And so the film may have the same effect on the diffusion of hydrogen. In Fig.10, the reactions occurred on the surface of the metal are as follow: $O_2 + 2H_2O + 4e = 4OH^-$(1) and $2H_2O + 2e = 2OH^- + H_2$ (2); Reaction (2) consists of two steps: $H_2O + e = OH^- + H$ (3) and $H + H = H_2$ (4) ; As to 16Mn steel without calcium deposits, the hydrogen generates by the reaction (2) and diffuses from the metal surface to solution quickly. But for the steel covered with calcium deposits, the diffusion of the hydrogen is suppressed because of calcium deposits. The hydrogen gathers on the surface of the metal and its concentration continues to increase. A high concentration of hydrogen inhibits reaction (4) directly and reaction (3) indirectly in turn; The hydrogen evolution reaction reduces, which means polarization potential should shift more negatively to maintain it. So the hydrogen evolution potentials shift negatively. At the same time, because of the diversity of thickness and integrity of calcium deposits films, the degree of obstruction for hydrogen evolution reaction differs and that is why hydrogen evolution potentials negatively move to different degrees.

As to the hydrogen permeation experiment, the mechanism above can explain it. The reaction of cathodic chamber is: $O_2 + 2H_2O + 4e = 4OH^-$(3) and $H_2O + e = OH^- + H(4)$; the reaction of anode chamber is: $H - e = H^+(5)$. The hydrogen atoms generate in cathodic chamber and adsorb on the surface of the metal. Most of them spread to the solution by the form of hydrogen molecule and the

rest diffuse to the metal. The hydrogen atoms move to the anode where they are oxidated to H^+ and at the same time some are bolted to the defect. As time goes on, hydrogen stuck in metal gradually saturates and more and more hydrogen atoms can diffuse to the anode quickly and then be oxidized. So the curve of hydrogen penetration current is increasing at the beginning until reaching the maximum point. For the steel without calcareous sediments, the concentration of the hydrogen atoms on the surface of the metal always keeps stable. According to the second diffusion mechanism, the rate of diffusion of hydrogen atoms will be stable and so the curve of hydrogen permeability current presents a platform; But for the steel covered with calcareous sediments, the calcareous sediments hinder the hydrogen molecule diffusing to the solution and therefore the concentration of hydrogen at the surface of 16Mn increases. The high concentration of hydrogen molecule inhibited reaction (4) directly and reaction (3) indirectly in turn and the hydrogen evolution reaction weaken. The formation rate of hydrogen atom reduces and its concentration decreases. Therefore, the diffusion rate of hydrogen atoms to the metal also decreases. So the hydrogen permeability current decline.

5. CONCLUSIONS

(1) Hydrogen evolution potentials of 16Mn steels covered with different calcium deposits shift negatively to different degrees.

(2) As pre-polarization potential shifts negatively, hydrogen evolution potential of 16Mn steels pre-treated turns negative constantly at first and then turns positive. The hydrogen evolution potential corresponding to pre-polarization potential at -1.05V is the lowest.

(3) The calcium deposits can inhibit the diffusion of hydrogen to solution directly and inhibit hydrogen evolution reaction indirectly, which results in hydrogen evolution potential of 16Mn steels covered with calcium deposits negatively shifting.

(4) The IR drop caused by calcium deposits can also let hydrogen evolution potential of 16Mn steels covered with calcium deposits negatively shift.

ACKNOWLEDGEMENTS

This research is supported by the Major State Basic Research Development Program of China (973 Program) (Granted No. 2014CB046805), National Natural Science Foundation of China (No.51131007, No. 51371124), the Key Project of Chinese Ministry of Education (No.11YJCZH202) and Natural Science Foundation of Tianjin (No. 14JCYBJC17700).

References

1. M. Chao, Q. Zheng, Q .W. Pang, *Corrostion&Protection*, 25 (2004) 473-488
2. S. Eliassen, *Corrosion Engineering science and technology*, 39(1) (2004) 31-37
3. J.X. Wu, Z.G. Fu, P.Q. Zhang, *Chin. Soc. Corros. Prot*, 9 (1989) 160-164
4. L. Bertolini, F. Bolzoni, P. Pedeferri, *Journal of applied electrochemistry*, 28 (1998) 1321-1331

5. Z.F. Li, F.X. Gan, X.H. Mao, *Corrosion Science*, 44 (2002) 689-701
6. S. Akonko, D.Y. Li, M. Ziomek-Moroz, *Tribology Letters*, 18(3) (2005) 405-410
7. F. Zucchi, V. Grassi, C. Monticelli, G. Trabanelli, *Corrosion Science*, 48 (2006) 522-530
8. Y. Liu, Y. Li, Q. Li, *Acta Metallurgica Sinica*, 49(9) (2013) 1089-1097
9. 9 W.C. Hooper, W.H. Hartt, *Corrosion*, 34(9) (1978) 320–323
10. X.H. Wang, C. Wang, X.H. Tang, Z.Z. Guo, *International Journal of Electrochemical Science*, 9(2014) 7660-7671
11. S.J. Kim, M. Okido, K.M. Moon, *Korean Journal of chemical engineering*, 20(3) (2003) 560-565
12. C.J. Li, M. Du, *Periodical of ocean university of china*, 41(7/8) (2011) 149–153
13. A. Neville, A.P. Morizot, *Journal of crystal growth*, 243 (2002) 490-502
14. C. Deslouis, D. Festy, O. Gil, *Electrochemical Acta*, 45 (2000) 1837–1845
15. Ch. Barchiche, C. Deslouis, D. Festy, *Electrochemical Acta*, 48 (2003) 1645–1654
16. C. Deslouis, D. Festy, O. Gil, *Electrochemical Acta*, 43 (1998) 1891–1901
17. N. Zhou, Y. Ding,L.Q. Ma, *Electroplating & pollution control*, 33(1) (2013) 4-6
18. J.J.M. Jebaraj, D.J. Morrison, I.I. Suni, *Corrosion Science*, 80(2014) 517-522
19. Z.M. Gao, Y.Y. Liu, F. Lin, *International Journal Of Electrochemical Science*, 8(2013) 10446-10453
20. D.H. Xia, Y.F. Sun, H.Q. Fan, *Transactions of Tianjin University*, 21 (2015) 554-561
21. D.H. Xia, Y.F. Sun, C. Shen, X.Y. Chen, H.Q. Fan, J.L. Luo, *Corrosion Science*, 100 (2015) 504-516
22. D.H. Xia, J.L. Luo, *Transactions of Tianjin University*, 21 (2015) 234-243
23. K.E. Mantel, W.H. Hartt, T.Y. Chen, *Corrosion*, 48(6) (1992) 489-499
24. W.H. Hartt, S.W. Smith, C.H. Culberson, *Corrosion*, 40(11) (1984) 609-618
25. A. Mujezinovic, A. Muharemovic, *High Performance & Optimum Design of Structure*, 137(2014) 509-517
26. C.J. Li, M. Du, J. Qiu, J. Zhang, *Acta metallurgica sinica*, 27(1) (2014) 131-139